

The two critical temperatures conundrum in $\text{La}_{1.83}\text{Sr}_{0.17}\text{CuO}_4$

Abhisek Samanta,^{1,*} Itay Mangel,^{2,†} Amit Keren,^{2,‡} Daniel P. Arovas,^{3,§} and Assa Auerbach^{2,¶}

¹*Department of Physics, The Ohio State University, Columbus OH 43210, USA*

²*Physics Department, Technion, 32000 Haifa, Israel*

³*Department of Physics, University of California at San Diego, La Jolla, CA 92093, USA*

(Dated: October 2, 2023)

The in-plane and out-of-plane superconducting stiffness appear to vanish at different transition temperatures, which contradicts thermodynamical expectation. In addition, we observe a surprisingly strong dependence of the out-of-plane stiffness transition on sample width. With evidence from Monte Carlo simulations, this effect is explained by a crossover from three dimensions into quasi one dimensional behavior of the finite sample. Due to an essential singularity at the thermodynamic transition temperature T_c , the out-of-plane stiffness *appears* to vanish below T_c by an amount which is proportional to the inverse width. A fit of our prediction to the data is used to determine the value of the anisotropy parameter. Analogy to studies of helium superfluids in nanopores is made.

A homogeneous three-dimensional superconductor is expected to exhibit a single transition temperature T_c at which the order parameter, $\Delta(T)$, and all the superconducting stiffness components vanish [1, 2]. In this regard, recent measurements of the ab -plane (ρ_{\parallel}) and c -axis (ρ_{\perp}) stiffnesses of $\text{La}_{1.83}\text{Sr}_{0.17}\text{CuO}_4$ crystals by Kapon *et. al.* [3] have been puzzling. Counter to the expectation above, ρ_{\perp} was seen to vanish at about 0.64 K below the vanishing temperature of ρ_{\parallel} .

The ‘stiffnessometer’ apparatus [4] comprised of a long excitation coil which pierces a superconducting ring. A bias current in the coil creates an Aharonov-Bohm vector potential A^{γ} which, by London’s equation, produces a persistent current that is measured by the induced magnetization m . Two rings, labelled by a and c , were prepared with their coil axes parallel (a) and perpendicular (c) to the CuO_2 planes. A measurement of $m > 0$ indicates a nonzero stiffness component ρ_{\parallel} or ρ_{\perp} for the c -or a -ring, respectively.

To better understand the different T_c ’s, this paper studies the effect of finite ring dimensions. We measure the a - and c -ring temperature-dependent relative magnetizations $m(T, L_a)/m_{\max}$, where m_{\max} is the zero temperature magnetization of the largest ring.

The rings were cut by a laser, or polished down to the geometries shown in Fig. 1(a-b). For the a -ring, we varied mostly the narrowest (bottleneck) widths of the $a-b$ planes, L_a , whereas for the c -ring we varied both L_c and L_a (see Figs. 1(a,b)). Fig. 1(c) shows the narrowest bottleneck geometry of the a -ring. Fig. 1(d) demonstrates visible dependence of the a -ring’s magnetization transition temperature on its width L_a . For comparison, the c -rings magnetization, depicted in Fig. 1(e), exhibits a width independent transition temperature, (except for the $L_a = 0.09$ mm sample, which is assumed to be damaged by a deep cut). More experimental details are given in the Supplementary Material (SM) [5].

The relative temperature shifts as a function of sample width are of order 1 – 10%, which are large and call

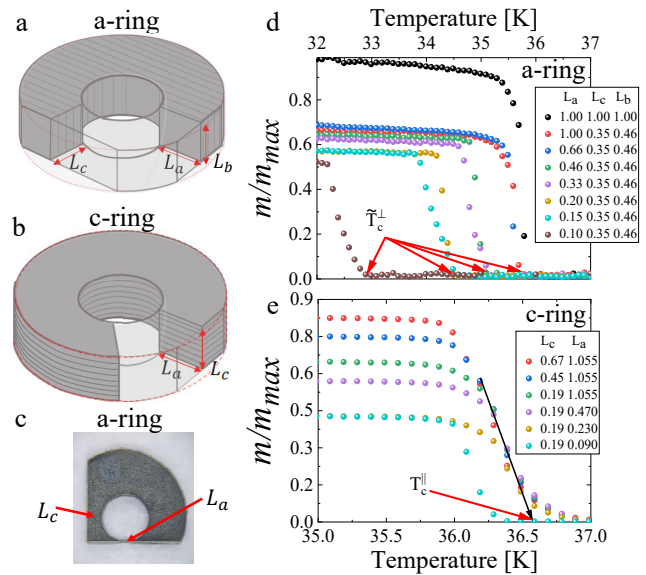


FIG. 1. Experimental configuration and magnetization data of $\text{La}_{1.83}\text{Sr}_{0.17}\text{CuO}_4$. (a) The interior of the a -ring with the CuO_2 plane parallel to the ring’s symmetry axis. This ring is cut along two planes and polished thus modifying three bottleneck lengths: L_a , L_b , and L_c . (b) The interior of the c -ring with the CuO_2 plane perpendicular to the ring’s symmetry axis. This ring is cut along one plane and polished, thus controlling two bottleneck lengths L_a and L_c . (c) Photograph of an a -ring with two cut planes. (d) Magnetization data of a -rings with different dimensions. (e) Magnetization data of c -rings with different dimensions. The mean transition temperature T_c^{\parallel} is defined by a linear extrapolation of $m(T)$ from below the correlated disorder-induced tail (see text). The narrowest sample $L_a = 0.09$, is suspected to contain a deep cut. m_{\max} stands for the $T \rightarrow 0$ magnetization of the largest ring.

for theoretical explanation. Two obvious options were considered:

(i) *Finite size effects of critical fluctuations are ruled out.* The correlation lengths are much smaller than mil-

limiter scale except unobservably near T_c [5–7].

(ii) *Disorder*. Short range uncorrelated disorder is not expected to affect the critical behavior of a superconductor, by Harris's criterion [8]. On the other hand, planar-correlated disorder, (or a gradient in dopant concentration along the c axis) [9, 10], leads to broadening of the ρ_{\parallel} transition with a high temperature tail. The same sample would have ρ_{\perp} vanish at a lower temperature than that of ρ_{\parallel} , which is determined by the planes with the smallest order parameters [5].

The experimental data of Fig. 1(e), indeed shows some effect of planar-correlated disorder. A high temperature tail of $\rho_{\parallel}(T)$ of width $\simeq 0.3\text{K}$ is seen above the linearly extrapolated magnetization data. However, we argue that correlated disorder alone cannot account for the systematic decrease of \tilde{T}_c^{\perp} with sample *width*, as seen in Fig. 1(d).

Below we show that the width dependent transition temperatures result from an *apparent* shift in the experimentally (and numerically) determined \tilde{T}_c^{\perp} 's which results from an essential singularity of ρ_{\perp} around its true transition temperature. This singularity is a consequence of two fundamental properties of cuprate superconductors:

(i) T_c is driven by phase fluctuations, as described by the classical XY model, rather than vanishing of the BCS gap [11]. This statement is supported by Uemura's empirical scaling of $T_c \propto \rho_{\parallel}$ [12], combined with the jump in ρ_{\parallel} at T_c which is observed in ultra-thin films [13].

(ii) Cuprates are layered superconductors with extremely high anisotropy between inter-layer and intralayer stiffness coefficients. The superconducting order parameter $\Delta(T)$ has a non-BCS, trapezoidal temperature dependence [14], which falls abruptly above the two dimensional Berezinskii-Kosterlitz-Thouless (BKT) temperature [15] as shown in Fig. 2.

In the crossover regime of $[T_{\text{BKT}}, T_c]$, a three dimensional sample with nearly cubic aspect ratio, crosses over to behave as a quasi one dimensional Josephson junction array along the c axis. The c -axis stiffness near T_c goes as $\rho_{\perp} \propto \exp(-K/\alpha L_a |T_c - T|^{2\beta})$, where $\alpha \ll 1$ is the anisotropy parameter, β is the order parameter's critical exponent. K is shown to be weakly (logarithmically) dependent on α and on the experimental cut-off which determines the apparent transition temperature \tilde{T}_c^{\perp} .

The analytic formulas for ρ_{\perp} and K are confirmed by fitting them to the Monte Carlo data for the stiffness coefficient of the three dimensional anisotropic XY model. The same expressions are applied to describe the data, and fitted them with a new (reasonable) estimate of its anisotropy parameter to $\alpha^{\text{fit}} = 3.4 \pm 1.5 \times 10^{-5}$.

In the summary we discuss the analogy between the quasi one dimensional behavior of layered cuprates, and (isotropic) superfluid density of ${}^4\text{He}$ embedded in quasi-

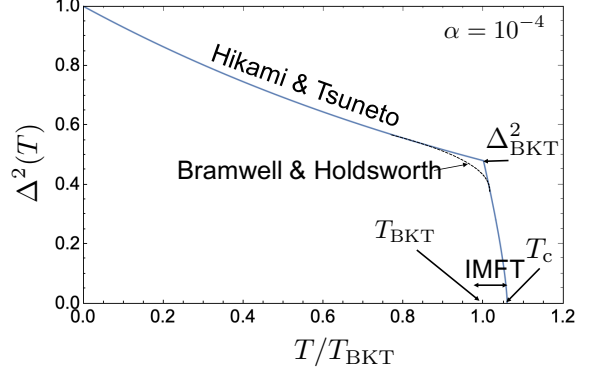


FIG. 2. The order parameter squared as a function of temperature for the layered classical XY model. The graph patches the linear spinwave theory of Hikami and Tsuneto [22], the crossover (dashed line) power law of Bramwell and Holdsworth [19], and the three dimensional critical point which is obtained by Interplane Mean Field Theory (IMFT) of Eqs. (2), (3) and (4).

one dimensional nanopores [16].

Model— We model the system by the three dimensional classical XY (3d XY) Hamiltonian on a tetragonal lattice,

$$H_{XY} = - \sum_i \sum_{\gamma} J_{\gamma} \cos(\varphi_{\mathbf{r}_i} - \varphi_{\mathbf{r}_i + \mathbf{a}_{\gamma}}) , \quad (1)$$

where $\gamma \in \{a, b, c\}$ and where $J_{a,b} = J_{\parallel}$ and $J_c = J_{\perp}$ are the effective intra- and inter-plane Josephson couplings. The anisotropy parameter $\alpha = J_{\perp}/J_{\parallel}$ will be fit to the experiments. Our temperature units are taken as $k_{\text{B}} = 1$. The effective lattice constants for the XY model's lattice are taken to be the Cooper-pair dimensions, as defined by the zero temperature coherence lengths $\xi_{\parallel,0}$ and $\xi_{\perp,0}$.

Decoupled layers ($\alpha = 0$) have a vanishing order parameter $\Delta = \langle e^{i\varphi} \rangle = 0$ but a finite in-plane stiffness up to the Berezinskii-Kosterlitz-Thouless [15] transition at $T_{\text{BKT}} \simeq 0.893 J_{\parallel}$. Interlayer mean field theory (IMFT) is applicable for high anisotropy $0 < \alpha \ll 1$ [14, 17–20]. It predicts a finite order parameter below the three dimensional critical temperature T_c which is slightly higher than T_{BKT} ,

$$\frac{T_c - T_{\text{BKT}}}{T_{\text{BKT}}} = \left(\frac{b}{|\ln(0.14\alpha)|} \right)^2 . \quad (2)$$

Here, the (non universal) constant is taken to be $b = 2.725$ [21].

In the regime $[0, T_{\text{BKT}}]$, the order parameter magnitude $\Delta = |\langle e^{i\varphi} \rangle|$ decreases from unity as calculated by Hikami and Tsuneto [22],

$$\Delta^2(T)_{T \leq T_{\text{BKT}}} \simeq \exp \left(-\frac{T \log(1/\alpha)}{4\pi J_{\parallel}} \right) . \quad (3)$$

Over the crossover regime $T \in [T_{\text{BKT}}, T_c]$, the order parameter squared initially crosses over with an intermediate power law of $|T - T^*|^{0.46}$, where $T^* = T_{\text{BKT}} + (T_c -$

$T_{\text{BKT}})/4$ [19], above which it drops precipitously toward T_c as,

$$\Delta^2(T) = m_{\text{BKT}}^2 t^{2\beta} \quad , \quad t \equiv \left(\frac{T_c - T}{T_c - T_{\text{BKT}}} \right) \quad , \quad (4)$$

where β crosses over from the mean field value $\frac{1}{2}$ to the 3dXY exponent 0.349, within a narrow three dimensional Ginzburg critical region of width $T_c / \log^4(\alpha)$ [14].

Fig. 2 depicts the smoothed “trapezoidal” temperature dependence of Δ^2 which differs from the BCS theory for the gap squared [14].

The superfluid stiffness components of the 3dXY model near criticality are

$$\rho_\gamma(T) = \rho_\gamma(T_{\text{BKT}}) t^s, \quad \gamma = a, b, c, \quad (5)$$

where s is the stiffness critical exponent given by [1]

$$s = 2\beta - \eta\nu \simeq 2\beta. \quad (6)$$

η and ν are the critical correlation function power law and correlation length exponents respectively. For the 3dXY model $\eta\nu = 0.0255$ which we henceforth neglect.

The *apparent* premature vanishing of ρ_\perp in a finite sample of an approximately unit aspect ratio, is due to its crossover to a quasi one-dimensional behavior as $T \rightarrow T_c$. The stiffness of a purely one dimensional (1d) classical XY model with Josephson coupling J_{1d} , lattice constant a and overall length L is given exactly by

$$\begin{aligned} \rho_{1d}(T, L) &= TLZ_2/Z_0 \\ Z_{2p} &= \sum_{n=-\infty}^{\infty} \left(\frac{I_n(J_{1d}/T)}{I_0(J_{1d}/T)} \right)^{L/a} n^{2p}, \end{aligned} \quad (7)$$

where I_n are modified Bessel functions and $p = 0, 1$. By Luttinger liquid (LL) theory [23, 24], for large $L \gg a$, ρ_{1d} depends on the scale variable $x \equiv LT/J_{1d} a$ as

$$\begin{aligned} \rho_{\text{LL}}(J_{1d}, x) &= J_{1d} a \left(1 - \frac{\pi^2}{x} \frac{\vartheta_3''(0, e^{-2\pi^2/x})}{\vartheta_3(0, e^{-2\pi^2/x})} \right) \\ &\simeq J_{1d} a \begin{cases} 1 & (x \leq 2) \\ 20 \exp(-0.472 x) & (x \geq 10) \end{cases} \end{aligned} \quad (8)$$

where $\vartheta_3(z, q) = 1 + 2 \sum_{n=1}^{\infty} q^{n^2} \cos(2nz)$, and prime denotes differentiation with respect to z . Comparison between Eqs. (7) and (8) is shown in the SM [5].

Strictly speaking $\rho_\perp(T, L_a)$ does not vanish at $T < T_c$. However, as $\Delta^2(T) \rightarrow 0$ decreases toward T_c , the layered superconductor crosses over to behave as an effectively quasi-1d array with an effective inter-plane coupling given by

$$J_{\text{eff}}(T) = \frac{L_a L_b}{\xi_{\parallel,0}^2} \times J_\perp \Delta^2(T), \quad (9)$$

where Δ^2 vanishes as $t^{2\beta}$ by Eq. (4). The geometric aspect ratio of the ring is defined as $r = L_c/L_b$ which is of order unity.

Inserting $x \rightarrow L_c T / (\xi_{\perp,0} J_{\text{eff}}(T))$ in the one dimensional expression of Eq. (8), the c -axis stiffness near $t \rightarrow 0$ goes as,

$$\rho_\perp(T) \approx 20 \rho_\perp(0) \exp\left(-\frac{K}{\alpha L_a} t^{-2\beta}\right) \quad , \quad (10)$$

where

$$K \simeq \frac{0.472 r T_c \xi_{\parallel,0}^2}{J_\parallel \Delta_{\text{BKT}}^2 \xi_{\perp,0}} \quad . \quad (11)$$

For any experimental resolution ε , an apparent vanishing temperature $\tilde{T}_c^\perp(\varepsilon)$ can be defined by equating

$$\rho_\perp(\tilde{T}_c^\perp) \equiv \varepsilon \rho_\perp(0) \quad . \quad (12)$$

By Eq. (10), the apparent width dependent transition temperature is,

$$T_c - \tilde{T}_c^\perp = (T_c - T_{\text{BKT}}) \left(\frac{K}{\alpha L_a \log(20/\varepsilon)} \right)^{1/2\beta} \quad (13)$$

The most important consequence of the quasi one-dimensional behavior, is that the temperature shifts are proportional to $(\alpha L_a)^{-1/2\beta}$. This is a much larger shift than expected from critical fluctuations, which are of order $(\alpha L_a^2)^{-1}$ [5].

Monte Carlo simulations – The superfluid stiffness (*i.e.* helicity modulus) of H_{XY} , with $a_\gamma = 1$, is given by [16, 25]

$$\begin{aligned} \rho_\gamma &= \frac{J_\gamma}{V} \left\langle \sum_{\langle ij \rangle} \cos(\varphi_{\mathbf{r}_i} - \varphi_{\mathbf{r}_j}) (r_i^\gamma - r_j^\gamma)^2 \right\rangle \\ &\quad - \frac{J_\gamma^2}{VT} \left\langle \left(\sum_{\langle ij \rangle} \sin(\varphi_{\mathbf{r}_i} - \varphi_{\mathbf{r}_j}) (r_i^\gamma - r_j^\gamma) \right)^2 \right\rangle, \end{aligned} \quad (14)$$

with $V = L_a L_b L_c$. The first contribution measures the short range correlations, which are proportional to minus the energy along the bonds in the γ direction. The second contribution measures long range current fluctuations, which vanish at zero temperature, and reduce the stiffness at finite temperatures.

To verify Eq. (13) we apply a Monte Carlo (MC) simulation of H_{XY} with the Wolff cluster updates algorithm [26]. We choose $L_c = L_b = 60$, and vary the width in the range $L_a \in \{40, 50, \dots, 80\}$ using the anisotropy parameters $\alpha = 0.01$ and 0.02 .

In Fig. 3, the MC results for $\rho_\perp(T)$ are shown. They exhibit qualitatively similar effects as seen experimentally, although numerics are restricted to much larger values of α and smaller sample sizes. The numerical data of

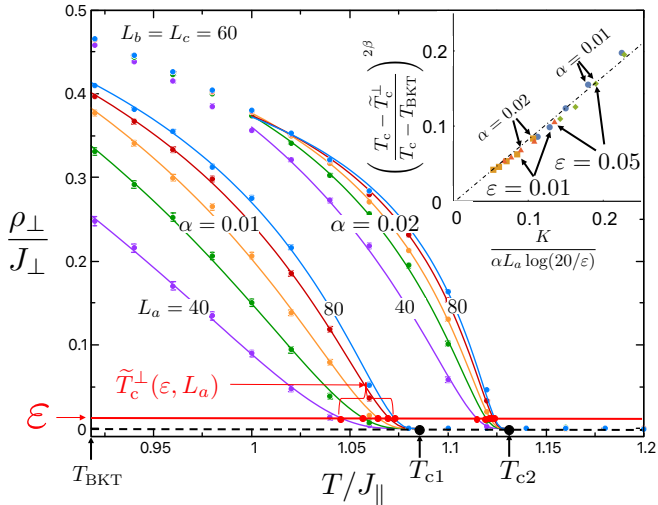


FIG. 3. MC evaluations of ρ_{\perp} as a function of temperature for a range of sample widths $L_a \in \{40, 50, \dots, 80\}$, and anisotropy parameters α . The thermodynamic critical temperatures are evaluated as $T_{c1} = 1.086J_{\parallel}$ and $T_{c2} = 1.13J_{\parallel}$ for $\alpha = 0.01$ and 0.02 , respectively. Solid lines are best fits to Eq. (10). ε is arbitrarily chosen as the numerical resolution which defines the apparent transition temperatures \tilde{T}_c^{\perp} by Eq. (12). Inset: Verification of Eq. (13) by collapsing of all the temperature shifts for various L_a, ε, α obtained from the main graphs.

$\rho_{\perp}(T)$ appear to vanish at temperatures which vary with L_a . A least squares fit of the MC data to the functional form given by Eq. (10), determines the apparent transition temperatures $\tilde{T}_c(L_a, \alpha, \varepsilon)$ for the choice of numerical resolution ε . In the inset we verify the validity of Eq. (13) by collapsing of all the temperature shifts onto a straight line. The slope of this line differs only by 20% from unity, which we attribute to the choice of the (non-universal) constants in the asymptotic expression of Eq. (8).

Note: In the SM [5], the numerical data of $\rho_{\parallel}(T)$ exhibits a tail *above* T_c . This tail exists even in the two dimensional limit $\alpha \rightarrow 0$ for finite planes. However, as mentioned earlier, such finite size effects cannot be observed at scale of the experimental samples' dimensions.

Comparison of theory to experiment – An experimental relative resolution of $\varepsilon = 10^{-2}$ determines the apparent transition temperature $\tilde{T}_c^{\perp}(L_a, \varepsilon)$ as the lowest temperature which obeys $m(T, L_a)/m_{\max} \leq \varepsilon$.

In Fig. 4, the transition temperature shifts in the a -rings are plotted versus L_a . The data is somewhat noisy, presumably because of introduction of deep cuts during the ring's cutting process, which are eliminated by subsequent cuts. To explain the experimental data we set the parameters of H_{XY} as follows. The lattice constants are taken as the zero temperature coherence lengths [14]

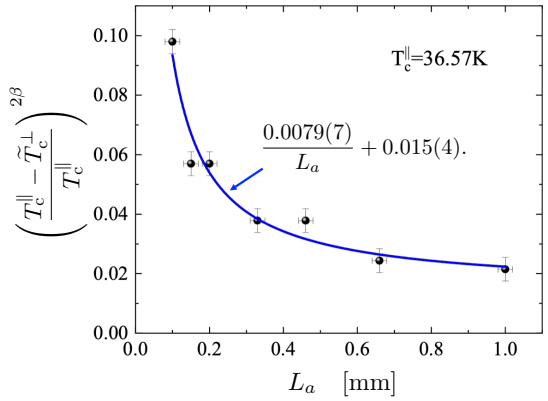


FIG. 4. Comparison of experiment and theory. Crosses: The apparent transition temperature shifts \tilde{T}_c^{\perp} and T_c^{\parallel} of $\text{La}_{1.83}\text{Sr}_{0.17}\text{CuO}_4$ from Fig. 1(d) and (e). L_a are the bottleneck widths of the ab planes in the a rings. Line: the least square fit which is used to determine $\alpha^{\text{fit}} = 3.4 \times 10^{-5}$, and the offset of the apparent transition temperature at infinite width, Eq. (19). Due to the narrow Ginzburg fluctuations regime, the mean field exponent $\beta = \frac{1}{2}$ is used for the fit.

estimated experimentally to be [27]

$$\xi_{\parallel,0} \simeq 3 \text{ nm} \quad , \quad \xi_{\perp,0} \simeq 1.3 \text{ nm} \quad . \quad (15)$$

The couplings are related to the zero temperature London penetration depths by the relations [14],

$$J_{\parallel} = \frac{\xi_{\perp,0}^2}{\lambda_a^2} \frac{\hbar^2 c^2}{16\pi e^2} \quad , \quad J_{\perp} = \frac{\xi_{\parallel,0}^2}{\xi_{\perp,0} \lambda_c^2} \frac{\hbar^2 c^2}{16\pi e^2} \quad . \quad (16)$$

e and c are the electron charge and the speed of light, respectively.

The a -ring is cut such that the induced current is confined effectively in a section of dimensions $L_b = 0.46$ mm, $L_c = 2$ mm, which yields $r = 4.34$. The width varies in the range $L_a \in [0.1, 1]$ mm. The minimal relative experimental resolution is $\varepsilon = 10^{-2}$. We find that the data of Fig. 4 can be fit by our Eq.(13) using

$$\alpha^{\text{fit}} = 3.4 \pm 1.5 \times 10^{-5}, \quad (17)$$

where the uncertainties are taken from the experimental error bars. By Eqs. (13) and (3),

$$\frac{T_c(\alpha) - T_{\text{BKT}}}{T_c} = 0.049 \quad , \quad m_{\text{BKT}}^2 = 0.44 \quad . \quad (18)$$

Using Eq. (17) we obtain $K = 0.257$ nm, which reproduces the coefficient of 0.0079 of the least squares fit in Fig. 4, with an offset of 0.015 for the transition temperatures of ρ_{\perp} at large width

$$\lim_{L_a \rightarrow \infty} \tilde{T}_c^{\perp} \approx 0.985 T_c^{\parallel} \quad . \quad (19)$$

This remnant relative difference in the large L_a limit, is attributed to correlated disorder, which is responsible for the tail of ρ_{\parallel} [5, 9, 10].

It should be pointed out that λ_c in $\text{La}_{1.83}\text{Sr}_{0.17}\text{CuO}_4$ was measured in Ref. [28] in magnetically oriented powder to be as large as $8.5\ \mu\text{m}$. In a low energy muon experiment on a single crystal [3], λ_c appeared to be too long to be detectable. Therefore, our stiffnessometer measurements can provide an alternate determination of λ_c in our crystal. We take the values $\lambda_a = 0.27\ \mu\text{m}$ from Ref. [29], and ξ_γ from Eq. (15). Using Eq. (16) and (17) yields

$$\lambda_c^{\text{fit}} = 21\ \mu\text{m} \quad (20)$$

for our samples.

Analog in ${}^4\text{He}$ – We have seen that $\alpha \ll 1$ can be mapped onto an isotropic model on samples with large aspect ratio. A similar “premature” vanishing of ρ_\perp has been observed on a quasi-one dimensional brick, *i.e.* $L_a \ll L_c$ [16]. This result was used to explain the experimental disappearance of superfluid density of ${}^4\text{He}$ embedded in quasi one-dimensional nanopores [30, 31]. Here we explain the *apparent* reduction of $\tilde{T}_c(L_a)$, not as a true thermodynamic transition but rather as a consequence of an essential singularity decay of ρ_\perp toward the thermodynamic T_c .

Acknowledgements – We thank Erez Berg, Snir Gazit, Dror Orgad, and Daniel Podolsky for beneficial discussions. AA acknowledge the Israel Science Foundation (ISF) Grant No. 2081/20. AK acknowledges the ISF Grant. No. 1251/19 and 3875/21. This work was performed in part at the Aspen Center for Physics, which is supported by National Science Foundation grant PHY-2210452, and at the Kavli Institute for Theoretical Physics, supported by Grant Nos. NSF PHY-1748958, NSF PHY-1748958 and NSF PHY-2309135.

* samanta.12@osu.edu
 † itaymangelsavir@gmail.com
 ‡ phkeren@technion.ac.il
 § darovas@ucsd.edu
 ¶ assa@physics.technion.ac.il

[1] M. E. Fisher, M. N. Barber, and D. Jasnow, *Phys. Rev. A* **8**, 1111 (1973).
 [2] M. Hasenbusch, *Phys. Rev. B* **100**, 224517 (2019).
 [3] I. Kapon, Z. Salman, I. Mangel, T. Prokscha, N. Gavish, and A. Keren, *Nat. Comm.* **10**, 2463 (2019).
 [4] I. Mangel, I. Kapon, N. Blau, K. Golubkov, N. Gavish, and A. Keren, *Phys. Rev. B* **102**, 024502 (2020).
 [5] “Supplementary Material.”
 [6] Y.-H. Li and S. Teitel, *Phys. Rev. B* **40**, 9122 (1989).
 [7] J. Cardy, *Finite-size scaling (Chapter 1)* (Elsevier, 2012).
 [8] A. B. Harris, *Jour. Phys. C: Sol. State Phys.* **7**, 1671 (1974).
 [9] P. Mohan, P. M. Goldbart, R. Narayanan, J. Toner, and T. Vojta, *Phys. Rev. Lett.* **105**, 085301 (2010).
 [10] D. Pekker, G. Refael, and E. Demler, *Phys. Rev. Lett.* **105**, 085302 (2010).
 [11] V. J. Emery and S. A. Kivelson, *Nature* **374**, 434 (1995).

[12] Y. J. Uemura, G. M. Luke, B. J. Sternlieb, J. H. Brewer, J. F. Carolan, W. N. Hardy, R. Kadono, J. R. Kempton, R. F. Kiefl, S. R. Kreitzman, P. Mulhern, T. M. Riseman, D. L. Williams, B. X. Yang, S. Uchida, H. Takagi, J. Gopalakrishnan, A. W. Sleight, M. A. Subramanian, C. L. Chien, M. Z. Cieplak, G. Xiao, V. Y. Lee, B. W. Statt, C. E. Stronach, W. J. Kossler, and X. H. Yu, *Phys. Rev. Lett.* **62**, 2317 (1989).
 [13] I. Hetel, T. R. Lemberger, and M. Randeria, *Nat. Phys.* **3**, 700 (2007).
 [14] A. Mihlin and A. Auerbach, *Phys. Rev. B* **80**, 134521 (2009).
 [15] J. M. Kosterlitz and D. J. Thouless, *Jour. Phys. C: Sol. State Phys.* **6**, 1181 (1973).
 [16] A. Kotani, K. Yamashita, and D. S. Hirashima, *Phys. Rev. B* **83**, 174515 (2011).
 [17] D. J. Scalapino, Y. Imry, and P. Pincus, *Phys. Rev. B* **11**, 2042 (1975).
 [18] B. Keimer, A. Aharony, A. Auerbach, R. J. Birgeneau, A. Cassanho, Y. Endoh, R. W. Erwin, M. A. Kastner, and G. Shirane, *Phys. Rev. B* **45**, 7430 (1992).
 [19] S. T. Bramwell and P. C. W. Holdsworth, *Phys. Rev. B* **49**, 8811 (1994).
 [20] P. Butera and M. Pernici, *Phys. Rev. B* **80**, 054408 (2009).
 [21] J. M. Kosterlitz, *Jour. Phys. C: Sol. State Phys.* **7**, 1046 (1974).
 [22] S. Hikami and T. Tsuneto, *Prog. Theor. Phys.* **63**, 387 (1980).
 [23] A. Del Maestro and I. Affleck, *Phys. Rev. B* **82**, 060515 (2010).
 [24] D. S. Hirashima, *Phys. Rev. B* **102**, 104506 (2020).
 [25] S. Teitel and C. Jayaprakash, *Phys. Rev. B* **27**, 598 (1983).
 [26] U. Wolff, *Phys. Rev. Lett.* **62**, 361 (1989).
 [27] I. Mangel and A. Keren, arXiv:2308.06757.
 [28] C. Panagopoulos, J. R. Cooper, T. Xiang, Y. S. Wang, and C. W. Chu, *Phys. Rev. B* **61**, R3808 (2000).
 [29] C. Panagopoulos, B. D. Rainford, J. R. Cooper, W. Lo, J. L. Tallon, J. W. Loram, J. Betouras, Y. S. Wang, and C. W. Chu, *Phys. Rev. B* **60**, 14617 (1999).
 [30] N. Wada, J. Taniguchi, H. Ikegami, S. Inagaki, and Y. Fukushima, *Phys. Rev. Lett.* **86**, 4322 (2001).
 [31] R. Toda, M. Hieda, T. Matsushita, N. Wada, J. Taniguchi, H. Ikegami, S. Inagaki, and Y. Fukushima, *Phys. Rev. Lett.* **99**, 255301 (2007).
 [32] F. Hrahsheh and T. Vojta, *Phys. Scripta* **2012**, 014074 (2012).
 [33] A. W. Sandvik, in *AIP Conference Proceedings*, Vol. 1297 (American Institute of Physics, 2010) pp. 135–338.

The two critical temperatures conundrum in $\text{La}_{1.83}\text{Sr}_{0.17}\text{CuO}_4$

Supplementary Material

For the anisotropic three dimensional XY model, we show that the finite size effects on the transition temperature are unobservably small, but planar correlated disorder produces a lower transition temperatures for ρ_{\perp} than for ρ_{\parallel} . The stiffness of the finite one dimensional XY chain is shown to asymptotically agree with the Luttinger liquid formula, used in the main text. We provide additional experimental details of the stiffness measurements, and numerical details of the Monte Carlo simulations.

ESTIMATION OF FINITE SIZE SHIFT IN T_c

Fine size scaling produce unobservably small finite size shifts of T_c for millimeter size samples, as shown by the following. The correlation lengths above T_{BKT} diverge as

$$\xi_{\parallel}(t) \simeq \frac{1}{\sqrt{\alpha}} \xi_a^{(0)} t^{-\nu}, \quad \xi_{\perp}(t) \simeq \xi_c^{(0)} t^{-\nu} \quad (21)$$

where we use the Ginzburg Landau definition of correlation lengths, $\xi_{\gamma}^{-1} \propto \sqrt{\rho_{\gamma}}$, to obtain the factor of $\sqrt{\alpha}$ between the divergent correlation length.

For Eq. (29) with sample dimensions $L_{\gamma}, \gamma = a, b, c$ the stiffness components near T_c vanish as [6],

$$\frac{\rho_{\perp}}{\rho_{\perp}(T_{\text{BKT}})} = t^{\nu} \Phi[x_a], \quad x_a = \xi_a(t)/L_a. \quad (22)$$

where $\Phi(x)$ is differentiable function with a finite value at $x = 0$. We expand Φ to linear order in ξ_a and set $\rho_{\perp} \rightarrow 0$ to obtain,

$$0 = \Phi_0 + \partial_{x_a} \Phi \times \left(\frac{t^{-\nu} \xi_a^{(0)}}{\sqrt{\alpha} L_a} \right) + \mathcal{O}(x_a^2) \quad (23)$$

which is solved by a positive shift of T_c by the amount

$$\delta t \simeq -\frac{\Phi_0}{\partial_a \Phi_{\gamma}} \left(\frac{\sqrt{\alpha} L_a}{\xi_a^{(0)}} \right)^{-\frac{1}{\nu}} \quad (24)$$

For the experimental $\text{La}_{1.83}\text{Sr}_{0.17}\text{CuO}_4$ rings, taking $\alpha = 10^{-5}$, $L_a/\xi_a^{(0)} \sim 10^6$, yields $|\delta t| \leq 10^{-4}$, which is much below experimental temperature resolution.

PLANAR CORRELATED DISORDER

Refs. [9, 10] have considered the layered XY model where the ab planes exhibit a variable z -dependent stiffness $\rho_{\parallel}(z)$ for $z \in [0, L_c]$. We can see the effects of this correlated disorder on systems with slow variation of $\rho_{\parallel}(z)$. In each segment, the critical behavior of the stiffness is

$$\rho_{\parallel}(T) = \rho_{\parallel}(0) |T - T_c^{\parallel}(z)|^{2\beta - \eta\nu} \quad (25)$$

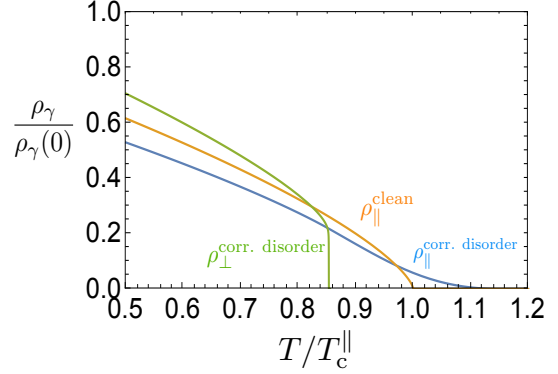


FIG. 5. Depiction of the effect of planar-correlated disordered $\rho_{\parallel}(z)$, with an average transition temperature T_c^{\parallel} and a width of transition temperatures $\delta T_c = 0.1 T_c^{\parallel}$. Orange line: The clean system with a three dimensional critical behavior. Blue line: the global $\rho_{\parallel}^{\text{cor. disorder}}$ showing a disorder induced high temperature tail above T_c^{\parallel} . Green line: the global $\rho_{\perp}^{\text{cor. disorder}}$, which is dominated by the weakest interplane stiffnesses, and vanishes below T_c^{\parallel} .

where $T_c^{\parallel}(z) \propto \rho_{\parallel}(z, 0)$ is the local transition temperature whose average is defined as T_c^{\parallel} and its variance is δT_c . The global ab -stiffness is given by the integral

$$\rho_{\parallel} = \rho_{\parallel}(0) \frac{1}{L_c} \int_0^{L_c} dz |T - T_c(z)|^{2\beta - \eta\nu} \quad (26)$$

which smears the average critical temperature T_c^{\parallel} by a high temperature tail of width δT_c .

In contrast, the c -axis stiffness $\rho_{\perp}(z)/\rho_{\perp}(0)$ is proportional to the local order parameter squared $\Delta(z)^2 = |T - T_c(z)|^{2\beta}$. The global c -axis stiffness is the harmonic average given by,

$$\rho_{\perp} = \frac{\rho_{\perp}(0)}{L_c} \left(\int_0^{L_c} dz \frac{1}{L_a^2 |T - T_c(z)|^{2\beta}} \right)^{-1} \quad (27)$$

The weakest segments (minimal $\rho_{\perp}(z)$), dominate the integral. In particular, at temperatures where some of the segments have vanishing $\Delta(T, z) = 0$, the whole integral vanishes. Therefore in effect, $\rho_{\perp}(T)$ identically vanishes at a lower temperature than T_c^{\parallel} . This is demonstrated

in Fig. 5, for a gaussian distribution of the T_c 's of $\rho_{\parallel}(z)$ and $\Delta^2(z)$, of width $\delta T_c = 0.1 T_c^{\parallel}$.

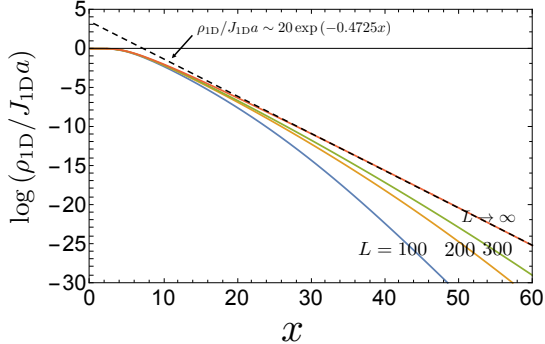


FIG. 6. Stiffness as a function of scaled variable $x = LT/(J_{1D}a)$ in the one dimensional XY model for different lengths L as given by the exact result of Eq. (7), and asymptotically at $L \rightarrow \infty$ by Eq. (8) of the main text.

ASYMPTOTIC BEHAVIOR OF STIFFNESS OF A ONE DIMENSIONAL XY CHAIN

In Fig. 6 we depict the exact result of the stiffness of the one dimensional XY chain as given by Eq. (7) of the main text. At large L/a the graphs show convergence to the analytic Luttinger-Liquid form [23, 24], which at large x is given by Eq. (8) of the main text.

EXPERIMENT

The experiment is base on a long excitation coil (EC) piercing a superconducting ring. At $T \rightarrow T_c$, the approximate London equation $j_{sc} = -\rho A_{ec}$, where j_{sc} is the current density in the coil and A_{ec} is the vector potential of the coil, ensures a finite current density in the ring. One then measures the magnetic moment of the ring m by moving a pickup loop relative to the ring and coil. The apparatus is shown in Fig. 7. For a perfect ring

$$m = h \int_{r_{in}}^{r_{out}} dr \pi r^2 j_{sc}(r) = -\frac{1}{4} \rho \Phi h (r_{out}^2 - r_{in}^2) \quad , \quad (28)$$

where h , r_{in} , and r_{out} are the ring's height, and inner and outer radii, and Φ is the flux produced by the coil. From these measurements, the stiffness can be extracted. For irregular rings the situation is more complicated, but the critical temperature of the stiffness is still measurable.

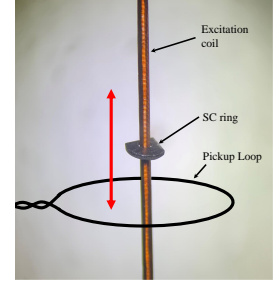


FIG. 7. A superconducting ring cut in two directions, on the excitation coil. The red double arrow shows the moving direction of the schematic pickup-loop relative to both coil and ring.

DETAILS OF THE MONTE-CARLO SIMULATIONS USING CLUSTER ALGORITHM

The Hamiltonian for the classical XY model on a tetragonal lattice is given by

$$H_{XY} = - \sum_{i,\gamma} J_{\gamma} \cos(\varphi_{\mathbf{r}_i} - \varphi_{\mathbf{r}_i + \mathbf{a}_{\gamma}}), \quad (29)$$

where $J_{a,b} = J_{\parallel}$, and $J_c = J_{\perp}$ are the effective intra-plane and inter-plane Josephson couplings respectively. $\alpha = J_{\perp}/J_{\parallel}$ is the ratio of inter-plane and intra-plane couplings or the anisotropy parameter used in the main text. The superfluid stiffness or the helicity modulus (with $a_{\gamma} = 1$) is given by [16, 25, 32]

$$\rho_{\gamma}(T) = \frac{J_{\gamma}}{V} \left\langle \sum_{\langle ij \rangle} \cos(\varphi_{\mathbf{r}_i} - \varphi_{\mathbf{r}_j}) (r_i^{\gamma} - r_j^{\gamma})^2 \right\rangle \quad (30)$$

$$- \frac{J_{\gamma}^2}{VT} \left\langle \left(\sum_{\langle ij \rangle} \sin(\varphi_{\mathbf{r}_i} - \varphi_{\mathbf{r}_j}) (r_i^{\gamma} - r_j^{\gamma}) \right)^2 \right\rangle,$$

where $V = L_a L_b L_c$ and $\langle ij \rangle$ corresponds to a bond involving sites i and j .

In the Wolff-cluster algorithm [26], we assume the XY spins \mathbf{S} to be the unit vectors in \mathbb{R}^3 . In every monte-carlo (MC) step, we first choose a random site $\mathbf{r} \in \mathbb{R}_3$ and a random direction $\mathbf{d} \in S_2$, and consider a reflection of the spin on that site about the hyperplane orthogonal to \mathbf{d} . Note that this is equivalent to the spin-flipping operation in Ising model. We then travel to all neighboring sites (\mathbf{r}') of \mathbf{r} , and check if the bond $\langle \mathbf{r} \mathbf{r}' \rangle$ is activated with a probability

$$P_{\gamma}(\mathbf{r}, \mathbf{r}') = 1 - \exp(\min[0, 2J_{\gamma}\beta(\mathbf{d} \cdot \mathbf{S}_{\mathbf{r}})(\mathbf{d} \cdot \mathbf{S}_{\mathbf{r}'})]), \quad (31)$$

where β is the inverse temperature. If this satisfies, we mark \mathbf{r}' and include it to a cluster \mathcal{C} of “flipped” spins. We iteratively continue this process for all unmarked neighboring sites of \mathbf{r}' and grow the cluster size until

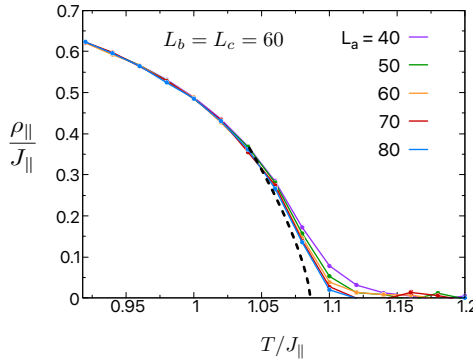


FIG. 8. The intra-plane helicity modulus or stiffness ρ_{\parallel} , plotted as a function of temperature T , for $\alpha = 0.01$ and for different L_a between 40 and 80, while L_b and L_c are kept fixed at 60. The error bars are also shown at every T , which are smaller than the point sizes. The black dashed line shows the expected thermodynamic behavior near the transition.

all the neighbors turn out to be marked. We use such 10^6 number of MC steps for thermalization, followed by another 10^7 number of MC steps for measurement of different observables, such as the helicity modulus and the binder cumulant. We estimate the errors of different observables by using a standard Jackknife analysis of the MC data.

In Fig. 3 of the Main text, we have presented the inter-plane superfluid stiffness ρ_{\perp} for different system sizes of $L_a \in [60 - 80]$, $L_b = L_c = 60$, near the transition. Here, in Fig. 8, we plot the intra-plane stiffness ρ_{\parallel} as a function of temperature T , for the same system sizes and for an anisotropic parameter $\alpha = 0.01$. We note that unlike ρ_{\perp} , ρ_{\parallel} falls to zero much more slowly. However, we observe that increasing system size (i.e. increasing L_a in Fig. 8) makes the vanishing of ρ_{\parallel} sharper. We expect that in the thermodynamic limit ρ_{\parallel} will also vanish exactly at T_c , shown in the ρ_{\perp} graphs of the main text. We therefore use a fitting function $f(T) = a(T_c - T)^{2\beta}$ between the temperature where the ρ_{\parallel} curves for different sizes start to deviate and the transition temperature

T_c (which is ~ 1.086 for these parameters) to show the expected thermodynamic behavior – this is shown by a dashed line in Fig. 8.

Next we calculate the binder cumulant, defined in terms of the higher powers of magnetization m as following [33]

$$U_2 = \frac{3}{2} \left(1 - \frac{1}{3} \frac{\langle m^4 \rangle}{\langle m^2 \rangle^2} \right), \quad (32)$$

and we use it to extract the value of critical temperatures accurately. As an example, in Fig. 9, we present U_2 as a function of T , for an anisotropy parameter $\alpha = 0.005$ and for different system sizes with a fixed aspect ratio $L_a = L_b$ and $L_a/L_c = 16$. In the ordered phase when all the spins are aligned it takes a value 1, while in the

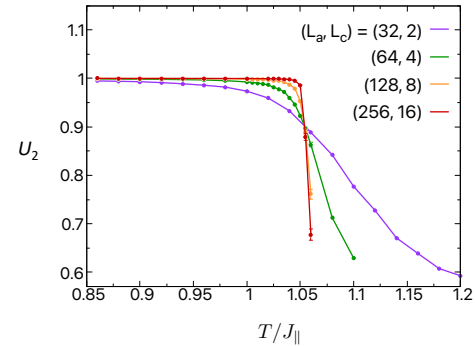


FIG. 9. Binder cumulant U_2 plotted as a function of temperature T , for anisotropy $\alpha = 0.005$ and for different sizes with a fixed aspect ratio $L_a/L_c = 16$ and $L_b = L_a$.

disordered phase it vanishes and takes an intermediate value between 0 and 1 at the critical point. Therefore, by tracking the crossing between different system sizes, we find a critical temperature $T_c \sim 1.05$ for these parameters. Using a similar analysis, we obtain T_c for other anisotropy parameters also, discussed in the main text.